

Stochastic Buffer-Aided Relay-Assisted MEC in Time-Slotted Systems

Javad Hajipour

Abstract—Mobile Edge Computing (MEC) is a promising paradigm to respond to the rising computation requests of the users in the emerging wireless networks, and especially in the Internet of Things (IoT). In this paper, we study buffer-aided relay-assisted MEC in systems with discrete transmission time-line and block fading channels. We consider a hierarchical network composed of a source, a buffer-aided relay, and another node in a higher level in the hierarchy. The source sends its tasks to the relay which in turn randomly assigns the received tasks to its own computing server or to the server of the next node in the hierarchy. We provide a framework to take into account the delays in both the transmission and computation buffers which facilitates the derivation of the expression for the Average Response Time (ART) in the system. Based on that and the system average power consumption in each slot, we introduce the concept of Average Response Energy (ARE) as a novel metric to capture the energy efficiency in MEC. Accordingly, we propose two offloading schemes with relevant problem formulations, namely the Minimum ART (MART) and the Minimum ARE (MARE) schemes, to optimize the ART or the ARE while keeping the system queues stable. We analyze the properties of the formulated problems, in terms of the feasible sets and the objective functions and noting them, we propose effective solution methods. Using extensive simulations, we validate the presented analysis and show the effectiveness of the proposed schemes in comparison with various baseline methods.

Index Terms—Mobile Edge Computing, Buffer-Aided Relaying, Task Computation Offloading, Convex Optimization.

I. INTRODUCTION

The advent of the Internet of Things (IoT) and the massive device connections in wireless networks have resulted in the proliferation of new applications utilized by these devices such as augmented reality, face recognition, and health-related applications. Consequently, the network providers have encountered new challenges to address the task computation requests from these devices in a timely manner. In this regard, Mobile Edge Computing (MEC) has emerged as a new approach to reduce the Average Response Time (ART) for the requested tasks by the IoT Devices (IoTDs) and other resource-constrained mobile stations [1]–[3]. In MEC, different components of the wireless networks are empowered with computing resources, which enable them to process the requested tasks by their own servers. This alleviates the need to send the tasks to the cloud servers located in distant data centers, and reduces the delay for the applications.

Many studies have investigated the potentials and challenges in this area while considering possible scenarios and

Javad Hajipour is with the Department of Computer Science at the University of Tabriz.

the related constraints. In particular, hierarchical computation architectures were studied in [4], [5], where a three-level hierarchy of computation facilities with two time scale model of frames and slots within each frame was considered in [4]. The authors proposed an auction-based policy for allocating the computation and communication resources in a way to maximize the service provider's profit in each frame and minimize the delay of the users in each slot. In [5], the ART of the users' requests was minimized by optimizing the cloudlet assignment and computation resource allocation. [6], [7] studied MEC systems in the presence of Intelligent Reflecting Surface (IRS) which is able to improve the signal propagation environment by configuring its reflecting elements in a way to enhance the signal reception quality at the receiver. [6] proposed an algorithm to jointly optimize the CPU frequency and transmit power of the IoTDs as well as the offloading time allocations and phase shifts of the IRS, in order to maximize the sum computational bits. [7] presented a combination of time-division multiple access (TDMA) and non-orthogonal multiple access (NOMA) as the data transmission scheme for the task offloading by the two users and minimized the sum delay of the users. [8] considered MEC in vehicular networks and maximized system utility for joint load balancing and offloading. In [9], a regional intelligent system for vehicular networks was presented using MEC. The authors considered different types of tasks and aimed at optimizing the resource allocation to minimize the delay. They formulated the problem as a Markov decision process and used deep Q-learning to address that. [10] studied a multi-user multi-server MEC system, where each user's task can be partitioned into several segments to be computed locally or assigned to edge servers, and a fairness-aware method was proposed to minimize the maximum delay for task computations in the system.

Energy efficiency is also one of the important challenges in Information and Communication Technology (ICT) management and hence, many works have investigated that in MEC systems. [11] studied energy efficient offloading scheme in TDMA and orthogonal frequency division multiple access (OFDMA) MEC systems in the presence of the users with the same delay constraint. The authors investigated the cases with infinite and finite computing capacity at the edge and proposed low-complexity algorithms to minimize the weighted sum energy consumption of the users. In [12], a multi-task scenario with sequential dependencies of the tasks was taken into account and the user association and computation offloading was designed to minimize the energy consumption. [13] studied energy efficient computation offloading in a time-slotted multi-user system by defining the computation efficiency as

the number of the computed bits divided by the corresponding energy consumption. The authors aimed at maximizing the computation efficiency while considering the constraints on the total energy of the devices, and proposed an iterative algorithm to obtain the optimal values for the processor speed and transmit power of the nodes as well as the slot portion allocation to different nodes. [14] studied energy and delay trade-off in a multi-user MEC system with a multi-antenna full-duplex (FD) base station (BS) that sends information in the downlink and receives computation task requests through the uplink transmissions of the users. The authors proposed a beamforming and power allocation scheme to minimize the weighted sum of the offloading energy and latency while considering constraints for maximum delay, maximum power and minimum signal-to-interference plus noise ratio (SINR).

These works mostly considered the hierarchy of the computing nodes as an architecture consisting of the servers at the wireless access nodes and the servers at the cloud computing centers. Even though they investigated many sophisticated scenarios, they did not take into account the various possibilities that can be brought by the relay nodes. But we note that, in the past decade, many works demonstrated the advantages of using relays, especially the buffer-aided relays, for improving the performance of the wireless networks [15]–[19]. In particular, [15] studied adaptive link selection in a three-node network comprising a source, a buffer-aided relay and a destination, and demonstrated significant throughput gains due to the use of buffer at the relay. A similar system was considered in [16] with fixed-rate and mixed-rate transmission scenarios, where the transmission rate at the source and relay are fixed or the relay adapts its transmission rate according to the channel state information, when available. For both cases, improvement in the throughput was observed. In [17], it was shown that buffer-aided relaying improves not only the throughput, but also the end-to-end delay. In fact, when considering the whole picture and taking into account the queuing delay at the source, it is revealed that the increase in system throughput leads to lower latency since the data arrival at the source until the reception at the destination. The advantages of buffer-aided relays were also demonstrated in the multi-user and multi-relay scenarios, e.g., [18] investigated energy efficiency gain in multi-user scenarios and [19] studied outage improvement in relay selection schemes in multi-relay networks.

Noting the aforementioned, there is a major research gap on using the relay nodes to enhance the MEC systems. Recently, in [20], a Multi-hop MEC (MMEC) architecture was proposed where it was shown that employing a computation capability at a buffer-aided relay and using a stochastic offloading scheme can improve the ART, significantly. But the results were derived based on the assumption that fixed transmission rates are used on the links; therefore, it was only applicable for the scenarios that the wireless channels do not experience deep fading and the transmitting nodes are able to adapt their transmit power according to the variations of the channel conditions. However, in practice, there are many scenarios that the wireless channels experience deep fading which does not permit successful transmission at some periods. Moreover, [20] assumed continuous time domain where the

nodes can start transmission/computation of a task whenever there is one in the corresponding transmission/computation buffers. However, many systems have discrete transmission time-line and the nodes are only allowed to transmit at the beginning of system-level defined time intervals. Thus, more investigations are required to analyze such systems, which are the subject of the current paper.

Specifically, in contrast to the existing works, we study stochastic buffer-aided relay-assisted MEC in the time-slotted systems with block fading channels, for the first time to the best of our knowledge. As for many new architectures and protocols, it is required to study the building blocks in the early stages of developing the relay-assisted MEC, to get clear insights about the effect of the fundamental parameters and the possible outcomes. Moreover, it is important to provide a framework which will give directions for investigating the next developments and the more sophisticated scenarios with different constraints. Hence, similar to [15]–[17], [20], we consider a three-node network as a building block of hierarchical time-slotted MMEC systems. It is composed of a source, a buffer-aided server-enabled relay, and another server-enabled node with a level higher than the level of the relay in the hierarchy, where the relay randomly decides to assign a received task to its own computing server or to offload the task to the next node. However, the presented discussions can be easily extended to MMEC systems with more than two hops and/or more than one source. We believe that the combination of MEC and buffer-aided relaying will play remarkable role in provisioning ubiquitous access to computation resources, in the emerging wireless networks densely populated with IoTs. In particular, buffer-aided relay-assisted MEC possesses promising potentials to exploit the ever-growing computation capabilities of the user equipments and/or relay nodes scattered in the wireless networks and to pave the way for high performance applications. Therefore, we are motivated to initiate the investigations in this area and build a solid basis for further research. In summary, the main contributions of this work are as follows:

- We present the system model and establish a framework to capture the factors affecting the ART in a time-slotted system with block fading channels and fixed transmit power on the links. In particular, we discuss the queuing model of the transmission buffers and derive their service probabilities.
- We analyze the ART in the system and compare its form with the counterpart in the continuous-time fixed-transmission-rate systems. Based on that, we propose the Minimum ART (MART) scheme with the problem formulation to find the optimal values for the transmit power on the links and the probability of task assignment to the relay, such that the lowest ART is achieved while keeping the system queues stable. We discuss the properties of the formulated problem and prove that the optimal value of the transmit power is equal to its maximum value. Then, we prove that the problem is convex with respect to the task assignment probability and therefore, it can be solved using a low-complexity one-dimensional search method.

- We demonstrate that at high values of the transmit power, increasing the power does not have much effect on the ART. We derive the Slot Average Power (SAP) as a function of the transmit power on the links and the task assignment probability. Based on that, we introduce a novel notion of energy efficiency as the product of the SAP and the ART in the system, yielding the concept of Average Response Energy (ARE). Using that, we propose the Minimum ARE (MARE) scheme and formulate a new optimization problem to obtain a low ART and at the same time use the system power efficiently. We explain the properties of the new objective function and provide directions to reduce the complexity of the solution strategies. Moreover, in the special case of Rayleigh fading, we demonstrate that the problem is convex with respect to the transmit power and based on that, we propose effective algorithms to find the optimal values of the transmit power and task assignment probability.
- We conduct extensive simulations to verify the presented analysis and also demonstrate the effectiveness of the proposed schemes in comparison with the related baseline methods. Moreover, we evaluate the performance of the proposed schemes in different system settings and provide valuable insights on the possible trends of the outcomes.

The rest of the paper is organized as follows. Section II describes the system model. In Section III, we present the proposed offloading schemes and the corresponding problem formulations. We analyze their properties and present the proposed solution methods. Numerical results are provided in Section IV, with the conclusion finally presented in Section V.

II. SYSTEM MODEL

We consider a three-node network, as shown in Fig. 1, comprising a Source Station (SS), a Relay Station (RS), and another node called the Higher-level Station (HS). The SS may represent an IoT or a wireless mobile station that does not have computing server. The RS and the HS may be respectively an installed wireless relay and the BS in a cellular network, or they may represent any wireless nodes in an ad hoc network that have computation capability and collaborate to process the tasks demanded by the SS. We assume that time is divided into the units of slot, where in each slot an application in the SS generates a task with arrival probability a and independent from other tasks. The SS stores the tasks in a transmission buffer to send to the RS whenever possible. On the other hand, the RS exploits a stochastic scheme to decide about processing or offloading the received tasks. In particular, when the RS receives a task, it assigns the task to its own computing server with probability ρ , and offloads the task to the HS with probability $1 - \rho$. The results of the tasks computed at the HS are sent back to the RS and join the results of the tasks computed by the RS, and they all are sent to the SS gradually.

There are separate dedicated orthogonal channels for transmissions on the SS-RS, RS-HS, HS-RS, and RS-SS links, and a direct SS-HS link does not exist. The RS has a computation buffer for storing the tasks to be computed by its own server. Moreover, it has a transmission buffer to store the tasks to be

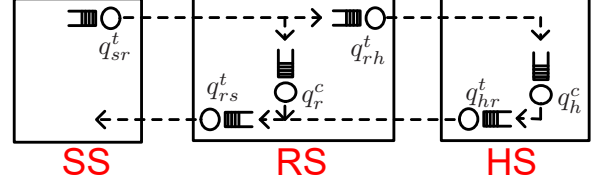


Fig. 1: System model.

forwarded to the HS and a transmission buffer to store the results to be sent to the SS. Similarly, the HS is equipped with two buffers, one for storing the tasks to be computed and another one for storing the results to be sent to the RS. At the beginning of each time slot, if there is a task/result in a transmission (computation) buffer and its serving channel (computation server) is available, the task/result is removed from the buffer and transmitted (computed) completely by the end of the slot. We assume that the propagation delay between the nodes is negligible. The response time for a task is defined as the time interval between the generation of the task at the SS and the reception of the result by the SS. Hence, this time interval consists of the waiting times at the transmission and computation buffers which in turn are affected by the service probabilities of the buffers. Based on the discussions above, the arrival and service processes of the buffers are Bernoulli processes and thus, the number of time slots between the arrivals and between the services of each buffer has geometric distribution. For such queuing systems with arrival probability x and service probability y , the queue is stable if $x < y$ [21]; in that case, the probability of a departure in a slot is also x and the average waiting time (in units of slot) is [22]:

$$W(x, y) = \frac{1 - x}{y - x}, \quad (1)$$

which includes the time spent in the queue and in the server of the queue.

We note that the computation servers of the RS and the HS may be busy due to processing their own tasks and hence, they may not be available in every time slot to process a task of the SS. The probability that in a time slot, the server of the RS (HS) can allocate its computation resources to process a task of the SS is denoted by q_r^c (q_h^c). On the other hand, sending the tasks/results from a transmission buffer is only possible in the slots that the signal-to-noise-ratio (SNR) at the receiver side of the serving link is higher than a threshold, γ . We assume that the channel conditions of the links are ergodic and stationary processes; they remain constant over one time slot but change from one slot to the next. Let g_{sr} , g_{rs} , g_{rh} , and g_{hr} denote the squared channel gains, respectively, on the SS-RS, RS-SS, RS-HS, and HS-RS links in a general time slot. We use $\mathcal{F}_{g_{sr}}(g)$ to denote the Cumulative Distribution Function (CDF) of g_{sr} which indicates the probability of having $g_{sr} \leq g$. $\mathcal{F}_{g_{rs}}(g)$, $\mathcal{F}_{g_{rh}}(g)$, and $\mathcal{F}_{g_{hr}}(g)$ are defined in a similar way. As an early work to combine MEC and buffer-aided relaying, we assume that all the nodes use identical and constant transmit power P . The reason for considering identical transmit power at all the nodes is that it allows to have similar transmission capability for all the nodes and focus only on the impact of the single power variable and the task assignment probability; however,

the problem formulations can be extended in future works to include the cases with different transmit powers at the nodes as well as other constraints.

Let N_0 denote the noise power at the receiver side of the links. The SNR on the SS-RS link is equal to $\frac{P_{g_{sr}}}{N_0}$; based on that and the aforementioned, the probability of having the SNR on the SS-RS link higher than γ , which indicates the probability of channel availability for successful task transmissions from the SS-RS transmission buffer, equals

$$q_{sr}^t(P) = 1 - \mathcal{F}_{g_{sr}}\left(\frac{\gamma}{P/N_0}\right). \quad (2)$$

$q_{rs}^t(P)$, $q_{rh}^t(P)$, and $q_{hr}^t(P)$ can be defined in a similar way. In the rest of the paper, we may refer to $q_{sr}^t(P)$, $q_{rs}^t(P)$, $q_{rh}^t(P)$, and $q_{hr}^t(P)$ as the channel service probabilities and, for brevity, we may omit the argument P in some equations. We assume that channel service probabilities are increasing functions of P , because as the transmit power increases, the probability of satisfying the threshold SNR, γ , at the receiver is increased.

Moreover, to be concrete, we will specialize the derived results for the case of Rayleigh fading channels. Noting the characteristics of Rayleigh distribution, we have $\mathcal{F}_{g_{sr}}(g) = 1 - e^{-\frac{g}{\bar{g}_{sr}}}$, where \bar{g}_{sr} is the mean value of g_{sr} . Thus, we obtain $q_{sr}^t = e^{-\frac{\Gamma_{sr}}{P}}$, where $\Gamma_{sr} = \frac{\gamma}{\bar{g}_{sr}/N_0}$. Similarly, for the RS-SS, RS-HS, and HS-RS links respectively, we have $q_{rs}^t = e^{-\frac{\Gamma_{rs}}{P}}$, $q_{rh}^t = e^{-\frac{\Gamma_{rh}}{P}}$, and $q_{hr}^t = e^{-\frac{\Gamma_{hr}}{P}}$, where Γ_{rs} , Γ_{rh} , and Γ_{hr} are defined similar to Γ_{sr} .

III. THE MART AND MARE SCHEMES

Based on the discussions in the previous section, in order to ensure queue stability, the service probability should be higher than the arrival probability for each queue. In that case, since the arrived tasks at the RS are randomly kept with probability ρ or offloaded to the HS with probability $1 - \rho$, the task arrival probability for the computation buffer at the RS will be ρa . For the RS-HS and HS-RS transmission buffers as well as the HS computation buffer, the task/result arrival probability will be $(1 - \rho)a$. Since the results of the tasks computed by the RS and HS enter the RS-SS transmission buffer, the arrival probability of the results at the RS-SS transmission buffer is a .

For the tasks computed by the RS, the ART consists of the waiting times in the SS-RS transmission buffer, the RS computation buffer, and the RS-SS transmission buffer. Hence, the ART of these tasks is obtained as

$$T_r(P, \rho) = W(a, q_{sr}^t) + W(\rho a, q_r^c) + W(a, q_{rs}^t) \quad (3)$$

Similarly, the ART of a task computed by the HS equals

$$T_h(P, \rho) = W(a, q_{sr}^t) + W((1 - \rho)a, q_{rh}^t) + W((1 - \rho)a, q_h^c) + W((1 - \rho)a, q_{hr}^t) + W(a, q_{rs}^t). \quad (4)$$

Hence, the ART of the tasks in the system is

$$T(P, \rho) = \rho T_r(P, \rho) + (1 - \rho) T_h(P, \rho). \quad (5)$$

Based on the aforesaid, we present two problem statements in the following with different objective functions; then, we discuss their properties and propose solution methods.

A. MART Scheme

We note that the ART equation derived in the previous section is different from that in [20]. In particular, due to the time-slotted nature of the current system and the queuing models, the numerators of the constituting terms of the ART are nonlinear (second-order polynomial) functions of ρ . Moreover, here, we also take into account the effect of transmit power on the ART, and we are interested to find the optimal transmit power, P^* , and the optimal probability of task assignment to the RS, ρ^* , that minimize the ART in the system. Specifically, we aim at addressing the following problem which is referred to as the MART problem:

$$\min_{P, \rho} T(P, \rho), \quad (6a)$$

$$\text{s.t. } C1 : a < q_{sr}^t(P), \quad (6b)$$

$$C2 : a < q_{rs}^t(P), \quad (6c)$$

$$C3 : (1 - \rho)a < q_{rh}^t(P), \quad (6d)$$

$$C4 : (1 - \rho)a < q_{hr}^t(P), \quad (6e)$$

$$C5 : \rho a < q_r^c, \quad (6f)$$

$$C6 : (1 - \rho)a < q_h^c, \quad (6g)$$

$$C7 : P \in [0, \hat{P}], \quad (6h)$$

$$C8 : \rho \in [0, 1], \quad (6i)$$

where, $C1 - C6$ state the stability conditions for the buffers of the system; $C7$ indicates that the maximum power a node can use is \hat{P} and $C8$ states the domain of ρ .

In general, problem (6) is not a convex optimization problem not least because constraints (6b)-(6e) cannot be stated in the form $f_i(P, \rho) \leq 0$ with $f_i(P, \rho)$'s being convex functions, due to the fact that $q_{sr}^t(P)$, $q_{rs}^t(P)$, $q_{rh}^t(P)$, and $q_{hr}^t(P)$ may not be concave functions of P (which is the case in particular for Rayleigh fading). Moreover, since the objective function (6a) is the sum of several nonlinear functions of P and ρ , getting its Hessian matrix is expensive and complicated; hence, it is difficult to verify the convexity of the objective function, even in the case of Rayleigh fading. Thus, in the following, we analyze the properties of problem (6) to obtain clues for finding P^* and ρ^* . We note that constraints (6b) and (6c) do not affect ρ and if they are satisfied for a given $P \in [0, \hat{P}]$, then the remaining constraints will determine the existence of feasible ρ .

Theorem 1. *For a given P that satisfies (6b), (6c) and (6h), problem (6) has feasible values for ρ if and only if*

$$\frac{q_r^c + \min(q_{rh}^t(P), q_h^c, q_{hr}^t(P))}{a} > 1, \quad (7)$$

and the set of feasible values for ρ is $\mathcal{A} = \mathcal{S} \cup (\max(0, 1 - \frac{\min(q_{rh}^t(P), q_h^c, q_{hr}^t(P))}{a}), \min(1, \frac{q_r^c}{a}))$, where

$$\mathcal{S} = \begin{cases} \{1, 0\} & \text{if } q_r^c > a, \min(q_{rh}^t(P), q_h^c, q_{hr}^t(P)) > a, \\ \{1\} & \text{if } q_r^c > a, \min(q_{rh}^t(P), q_h^c, q_{hr}^t(P)) = a, \\ \{0\} & \text{if } q_r^c = a, \min(q_{rh}^t(P), q_h^c, q_{hr}^t(P)) > a, \\ \{\} & \text{otherwise.} \end{cases} \quad (8)$$

Proof. This can be proved easily similar to the first theorem in [20]. \square

In the following theorem, $I(x)$ is unit step function defined to be one if $x > 0$ and zero otherwise.

Theorem 2. *If problem (6) is feasible, then $P \in (\check{P}, \hat{P}]$, where $\check{P} = \max(\check{P}_1, \check{P}_2) < \hat{P}$, $\check{P}_1 = \max(q_{sr}^{t-1}(a), q_{rs}^{t-1}(a))$, $\check{P}_2 = I(a - q_r^c) \max(q_{rh}^{t-1}(a - q_r^c), q_{hr}^{t-1}(a - q_r^c))$, where superscript “ -1 ” for a functions indicates the inverse of that function. In the special case of Rayleigh fading channels, $\check{P}_1 = -\frac{\max(\Gamma_{sr}, \Gamma_{rs})}{\ln a}$, $\check{P}_2 = -I(a - q_r^c) \frac{\max(\Gamma_{rh}, \Gamma_{hr})}{\ln(a - q_r^c)}$.*

Proof. If the problem is feasible, there exists P and ρ that satisfy the constraints. Based on (6b) and (6c), we have $\min(q_{sr}^t(P), q_{rs}^t(P)) > a$ which is equivalent to $P > \check{P}_1 = \max(q_{sr}^{t-1}(a), q_{rs}^{t-1}(a))$. Moreover, based on (7), we have $\min(q_{rh}^t(P), q_h^c, q_{hr}^t(P)) > a - q_r^c$; this necessitates $\min(q_{rh}^t(P), q_{hr}^t(P)) > a - q_r^c$ which holds for any $P > 0$ if $a - q_r^c \leq 0$, and for $P > \max(q_{rh}^{t-1}(a - q_r^c), q_{hr}^{t-1}(a - q_r^c))$ if $a - q_r^c > 0$; these two cases can be concisely stated as $P > \check{P}_2 = I(a - q_r^c) \max(q_{rh}^{t-1}(a - q_r^c), q_{hr}^{t-1}(a - q_r^c))$. Hence, $P > \check{P} = \max(\check{P}_1, \check{P}_2)$. Noting (6h), we conclude that $\check{P} < P \leq \hat{P}$. For Rayleigh fading channels, by substituting the corresponding equations for the channel service probabilities, we get $\check{P}_1 = -\frac{\max(\Gamma_{sr}, \Gamma_{rs})}{\ln a}$, $\check{P}_2 = -I(a - q_r^c) \frac{\max(\Gamma_{rh}, \Gamma_{hr})}{\ln(a - q_r^c)}$. \square

For conciseness, in the following theorem we use $q_{rh}^t(P)$ to refer to $\min(q_{rh}^t(P), q_{hr}^t(P))$.

Theorem 3. *By increasing P from \check{P} towards \hat{P} , one of the following cases will occur for the size of \mathcal{A} :*

- *H1: It does not change, if $q_{rh}^t(\check{P}) \geq \min(q_h^c, a)$.*
- *H2: It continuously increases, if $q_{rh}^t(\hat{P}) \leq \min(q_h^c, a)$.*
- *H3: It continuously increases as P increases from \check{P} up to $\check{P} = \max(q_{rh}^{t-1}(\min(q_h^c, a)), q_{hr}^{t-1}(\min(q_h^c, a)))$ and then it does not change, if $q_{rh}^t(\hat{P}) < \min(q_h^c, a)$ and $q_{rh}^t(\hat{P}) > \min(q_h^c, a)$. In the case of Rayleigh fading, $\check{P} = -\frac{\max(\Gamma_{rh}, \Gamma_{hr})}{\ln(\min(q_h^c, a))}$.*

Proof. According to Theorem 1, the upper boundary of \mathcal{A} is independent from P and the lower boundary depends on $\min(q_h^c, q_{rh}^t)$. Based on Theorem 2, q_{rh}^t is minimum at \check{P} and maximum at \hat{P} , as q_{rh}^t and q_{hr}^t are increasing functions of P . Hence, we have the following cases:

- If $q_{rh}^t(\check{P}) \geq \min(q_h^c, a)$, either $a > q_h^c$ and $q_{rh}^t(\check{P}) \geq q_h^c$ and hence, the lower boundary of \mathcal{A} is determined by $1 - \frac{q_h^c}{a}$, or $q_h^c \geq a$ and $q_{rh}^t(\check{P}) \geq a$ and hence, the lower boundary of \mathcal{A} is 0. In either case, the lower boundary is independent from q_{rh}^t , q_{hr}^t and P . This remains true as P increases and hence, case H1 holds.
- If $q_{rh}^t(\hat{P}) \leq q_h^c$ and $q_{rh}^t(\hat{P}) \leq a$, the lower boundary of \mathcal{A} is determined by $1 - \frac{q_{rh}^t(\hat{P})}{a}$ for any $P \in (\check{P}, \hat{P}]$. Therefore, as P increases in that interval, $q_{rh}^t(P)$ increases and the lower boundary of \mathcal{A} decreases and hence, the size of \mathcal{A} increases. Therefore, case H2 holds.
- If none of the conditions above holds, then $q_{rh}^t(\check{P}) < q_h^c$ and $q_{rh}^t(\hat{P}) < a$ but $q_{rh}^t(\hat{P}) > q_h^c$ or $q_{rh}^t(\hat{P}) > a$. In this situation, at low values of $P \in (\check{P}, \hat{P}]$, $q_{rh}^t(P)$ determines the lower boundary of \mathcal{A} . Hence, as P increases, $q_{rh}^t(P)$ increases and the lower boundary decreases and

the size of \mathcal{A} increases; but this continues up to the point that $q_{rh}^t(P)$ equals q_h^c or a , whichever happens first, i.e., up to $\hat{P} = \max(q_{rh}^{t-1}(\min(q_h^c, a)), q_{hr}^{t-1}(\min(q_h^c, a)))$, because after that point, either q_h^c determines the lower boundary or the lower boundary is 0. This proves case H3. For Rayleigh fading, exploiting the equations for channel service probabilities, we have $\check{P} = -\frac{\max(\Gamma_{rh}, \Gamma_{hr})}{\ln(\min(q_h^c, a))}$. \square

Theorem 4. *P^* is equal to \hat{P} .*

Proof. Let $\hat{\mathcal{S}}$ denote the feasible set of ρ at $P = \hat{P}$. For any $\rho \in \hat{\mathcal{S}}$, decreasing the P will decrease q_{sr}^t , q_{rs}^t , q_{rh}^t , q_{hr}^t and hence, according to Theorems 1-3, the problem may remain feasible or not; but according to (5), the objective function will certainly increase. This concludes the theorem. \square

The abovementioned theorem can be explained as follows. As P increases, the right-hand sides of the constraints (6d) and (6e) increase, which allow for a larger range of feasible ρ and therefore, the possibility for a ρ with lower ART increases. Moreover, the higher the P , the lower the waiting times at the transmission buffers.

Based on the insights gained by the discussions above, problem (6) can be transformed to a single-variable convex optimization problem. For that, the channel service probabilities should be calculated using $P^* = \hat{P}$, and substituted in the problem.

Theorem 5. *For a given P , in particular for P^* , problem (6) is a convex optimization problem with respect to ρ .*

Proof. For a given P , channel service probabilities are constant and the constraints of problem (6) are linear functions with respect to ρ . Hence, it is only needed to prove the convexity of the objective function by showing that its second derivative is positive [23]. (1)-(5) indicate that the objective function is the sum of the functions having the forms $f_0 = \frac{1-a}{q_0-a}$, $f_1(\rho) = \frac{\rho-\rho^2 a}{q_1-\rho a}$ and $f_2(\rho) = \frac{(1-\rho)-(1-\rho)^2 a}{q_2-(1-\rho)a}$, where q_0 , q_1 , and q_2 represent the symbols for transmission/computation service probabilities in the different function forms and f_0 is a constant function with respect to ρ . The second derivatives of $f_1(\rho)$ and $f_2(\rho)$ are as follows:

$$f_1''(\rho) = \frac{2aq_1(1-q_1)}{(q_1-\rho a)^3}, \quad f_2''(\rho) = \frac{2aq_2(1-q_2)}{(q_2-(1-\rho)a)^3}. \quad (9)$$

It is clear that the values of a , q_1 , and q_2 are in the interval $(0, 1]$ and, according to the constraints, $(q_1 - \rho a) > 0$, $(q_2 - (1 - \rho)a > 0)$ for feasible values of ρ . Therefore, $f_1''(\rho) > 0$ and $f_2''(\rho) > 0$ and hence, $f_1(\rho)$ and $f_2(\rho)$ are convex functions. Noting that the sum of convex and constant functions is a convex function, it is inferred that for a given P and in particular for P^* , the objective function (6a) is convex with respect to ρ . \square

According to Theorem 5, after substituting the channel service probabilities (at $P^* = \hat{P}$) in the problem, the resulted problem will be a single-variable convex optimization problem with respect to ρ . Therefore, ρ^* can be found easily by using an efficient one-dimensional search such as the Golden

section method [23], which has the computational complexity of $O(\log(1/\delta))$, where δ is the desired relative error bound. This method can be easily implemented in the RS or the HS as they both have computation capability.

B. MARE Scheme

In many scenarios, we are interested to have a low ART, not necessarily the minimum one, and at the same time use the system energy efficiently. To clarify that, Fig. 2 illustrates the ART with respect to ρ for different values of P , in a system with $a = 0.01$, $q_r^c = q_h^c = 0.015$, and Rayleigh fading with $\Gamma_{sr} = \Gamma_{rs} = \Gamma_{rh} = \Gamma_{hr} = 0.01$. It is observed that for any ρ , when P is increased from 3 mW to 6 mW, there is a significant improvement in the ART; but when P is increased more, the ART does not change much. In other words, the Rate of Decrease (RoD) in the ART is very smaller than the Rate of Increase (RoI) in energy consumption.

Noting the aforementioned, we are motivated to strike a balance between the energy consumption in the system and the response time of the tasks. We know that the energy consumption on a link is proportional to the average power consumption of that link in each slot. On the other hand, the average power consumption of a link is proportional to the ratio of the time slots that there is a transmission on that link. Hence, the average power consumptions in each slot on the SS-RS, RS-SS, RS-HS, and HS-RS links are respectively equal to aP , aP , $(1-\rho)aP$, and $(1-\rho)aP$. We define the SAP in the system as the sum of the average power consumptions of all the links in each slot, i.e.,

$$\bar{P}_s(P, \rho) = 2(2-\rho)aP. \quad (10)$$

In order to use the system energy efficiently, we take into account both the RoI in the energy consumption and the RoD in the ART and define a novel objective function as the product of the SAP and the ART in the system. This product can be interpreted as the average energy consumption during the response time of the tasks. Thus, we refer to it as the ARE, denoted by

$$E(P, \rho) = \bar{P}_s(P, \rho)T(P, \rho), \quad (11)$$

and propose the MARE offloading scheme with the following optimization problem:

$$\min_{P, \rho} E(P, \rho), \quad (12a)$$

$$\text{s.t. } C1 - C8. \quad (12b)$$

Similar to the MART problem, in general, the MARE problem is not a convex optimization problem. It is clear that Theorems 1-3 hold also for the MARE problem, since it has the same constraints as the MART problem. However, due to the multiplication of $(2-\rho)P$ and $T(P, \rho)$ terms in the objective function, neither of Theorems 4 and 5 are applicable for the MARE problem. Therefore, another numerical method should be used to find P^* and ρ^* . Even, running an exhaustive search with a desired precision over two dimensions of P and ρ is not very expensive, computationally, for two reasons. First, it is only over two dimensions. Second, the problem is

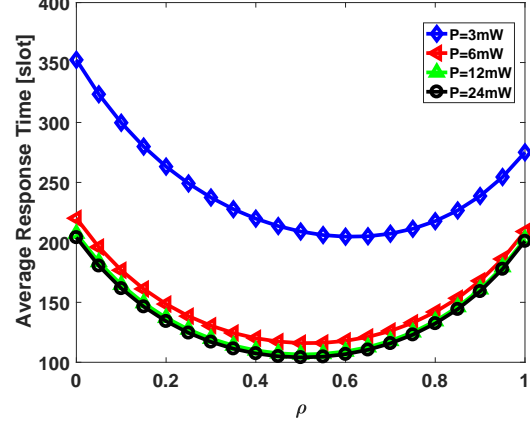


Fig. 2: Effect of different values of P on the ART in a system with $a = 0.01$, $q_r^c = q_h^c = 0.015$, and Rayleigh fading with $\Gamma_{sr} = \Gamma_{rs} = \Gamma_{rh} = \Gamma_{hr} = 0.01$.

only needed to be solved once, i.e., at the beginning of the operation, not in every time slot; after that, all the nodes will use P^* for their transmissions and the RS will work based on ρ^* whenever it receives a task from the SS. However, reducing the needed steps for solving a problem is always desirable. In the following, we discuss the properties of the objective function with respect to ρ in general and with respect to P in the especial case of Rayleigh fading; these provide directions to reduce the number of iterations for searching the solution of the MARE problem.

Remark 1: For a given P , the constraints of the MARE problem are linear with respect to ρ . The objective function $E(P, \rho)$ is the sum of the linear decreasing functions $(2-\rho)aPW(a, q_{sr}^t)$, $(2-\rho)aPW(a, q_{rs}^t)$, and the rational functions having the forms $f_3 = aP(2-\rho)\rho^{\frac{1-\rho a}{q_3-\rho a}}$ and $f_4 = aP(2-\rho)(1-\rho)\frac{1-(1-\rho)a}{q_4-(1-\rho)a}$. The derivatives of f_3 and f_4 with respect to ρ can be obtained respectively as

$$f_3' = 2aP(1-\rho) \left[\frac{1-\rho a}{q_3-\rho a} + \frac{\rho a(1-q_3)}{(q_3-\rho a)^2} \right], \quad (13a)$$

$$f_4' = aP \left[\frac{(2\rho-3)(1-(1-\rho)a)}{q_4-(1-\rho)a} + (2-\rho)(1-\rho)a \frac{q_4-1}{(q_4-(1-\rho)a)^2} \right]. \quad (13b)$$

Since $\rho \leq 1$, $q_3 \leq 1$, $q_4 \leq 1$, $\rho a < q_3$ and $(1-\rho)a < q_4$, we notice that $f_3' \geq 0$ and $f_4' \leq 0$. Thus, for a given P , $E(P, \rho)$ is the sum of increasing rational functions and decreasing rational/linear functions with respect to ρ . Hence, we expect $E(P, \rho)$ to be either increasing or decreasing or convex or concave function of ρ , depending on the effect of its decreasing and increasing terms. Consequently, for a given P , we expect $E(P, \rho)$ to have its minimum at one of the boundaries of \mathcal{A} or to have at most a single local minimum point inside \mathcal{A} which can be found using an efficient one-dimensional search, like Golden section method, over ρ . We have verified this through function plots with many different parameter settings. However, it cannot be proved analytically. Therefore, for high reliability, the domain of ρ can be partitioned into several sub-domains for each of which, a local optimal point can be found, and the minimum among all of them can be chosen

Algorithm 1 K -Partition Search Over ρ

```

1: set  $\varphi = \frac{3-\sqrt{5}}{2}$ ,  $k = 1$ ;  $P$ ,  $K$  and  $\delta$  as intended.
2: calculate  $q_{sr}^t$ ,  $q_{rs}^t$ ,  $q_{rh}^t$  and  $q_{hr}^t$  using  $P$ .
3: set  $\rho_l = \max(0, 1 - \frac{\min(q_{sr}^t, q_h^c, q_{hr}^t)}{a})$ ,  $\rho_u = \min(1, \frac{q_h^c}{a})$ 
4: if  $\min(q_{rh}^t, q_h^c, q_{hr}^t) \leq a$ ,  $\rho_l = \rho_l + \delta$ .
5: if  $q_r^c \leq a$ ,  $\rho_u = \rho_u - \delta$ .
6:  $\rho^* = \rho_l$ .
7: while  $k \leq K$ 
8:    $\rho_1 = \rho_l + \frac{\rho_u - \rho_l}{K}(k - 1)$ ,  $\rho_4 = \rho_l + \frac{\rho_u - \rho_l}{K}k$ 
9:   while  $\rho_4 - \rho_1 > \delta$ 
10:     $\rho_2 = \rho_1 + \varphi(\rho_4 - \rho_1)$ ,  $\rho_3 = \rho_4 - \varphi(\rho_4 - \rho_1)$ .
11:    if  $E(P, \rho_2) < E(P, \rho_3)$ ,  $\rho_4 = \rho_3$ ; else  $\rho_1 = \rho_2$ .
12:   end while
13:   if  $E(P, \frac{\rho_1 + \rho_4}{2}) < E(P, \rho^*)$ ,  $\rho^* = \frac{\rho_1 + \rho_4}{2}$ .
14:    $k = k + 1$ .
15: end while
16: return  $\rho^*$ .

```

Algorithm 2 MARE Algorithm in General Cases

```

1: set  $K$  and  $\delta$  as intended.
2: initialize  $P^* = P_x = \check{P} + \delta$ , with  $\check{P}$  defined in Theorem 2.
3: use Algorithm 1 with  $P = P_x$ ; store the output in  $\rho^*$ .
4: while  $P_x \leq \hat{P}$ 
5:   use Algorithm 1 with  $P = P_x$ ; store the output in  $\rho_x$ .
6:   if  $E(P_x, \rho_x) < E(P^*, \rho^*)$ , then  $P^* = P_x$ ,  $\rho^* = \rho_x$ .
7:    $P_x = P_x + \delta$ .
8: end while
9: return  $P^*$  and  $\rho^*$ .

```

as the near-optimal point. For clarification, this is presented in Algorithm 1 where K is the intended number of partitions over the domain of ρ .

To summarize, Algorithm 2 shows the whole procedure for solving the MARE problem, which is a combination of exhaustive search and Golden section method. The exhaustive search is done over the domain of P and at each step, Algorithm 1 is utilized to obtain the best ρ at the given P . Therefore, Algorithm 2 has the computational complexity of $O(\frac{K}{\delta} \log(1/\delta))$.

Theorem 6. *In the case of Rayleigh fading, for a given ρ , problem (12) is a convex optimization problem with respect to P .*

Proof. Let substitute the channel service probabilities in the constraints (6b)-(6e) with their equations in terms of P in the case of Rayleigh fading. Then, it is observed that the constraints of the problem have the nonlinear form $c_1a < e^{-\frac{\Gamma}{P}}$, where c_1 is either 1 or $(1-\rho)$, and Γ is one of Γ_{sr} , Γ_{rh} , Γ_{hr} , and Γ_{sr} which are positive constants. By taking the logarithm of the two sides of the constraints, they can be transformed into

Note that lines 9-12 of Algorithm 1 implement the iterations of the Golden section method for each sub-domain of ρ . Hence, Algorithm 1 can also be used to solve the MARE problem, by setting $K = 1$, $P = P^*$, and using $T(P, \rho)$ instead of $E(P, \rho)$.

Algorithm 3 MARE Algorithm in Rayleigh Fading

```

1: set  $\varphi = \frac{3-\sqrt{5}}{2}$ ,  $K$  and  $\delta$  as intended.
2: initialize  $P_1 = \check{P} + \delta$  and  $P_4 = \hat{P}$ , with  $\check{P}$  defined in Theorem 2.
3: while  $P_4 - P_1 > \delta$ 
4:    $P_2 = P_1 + \varphi(P_4 - P_1)$ ,  $P_3 = P_4 - \varphi(P_4 - P_1)$ .
5:   use Algorithm 1 with  $P = P_2$ ; store the output in  $\rho_1$ .
6:   use Algorithm 1 with  $P = P_3$ ; store the output in  $\rho_2$ .
7:   if  $E(P_2, \rho_1) < E(P_3, \rho_2)$ 
8:      $P_4 = P_3$ 
9:   else
10:     $P_1 = P_2$ 
11:   end if
12: end while
13: set  $P^* = \frac{P_1 + P_4}{2}$ ; use Algorithm 1 with  $P = P^*$  and store the output in  $\rho^*$ .
14: return  $P^*$  and  $\rho^*$ .

```

the equivalent linear forms $P < -\frac{\Gamma}{\ln c_1 a}$. Hence, it is sufficient to prove the convexity of the objective function $E(P, \rho)$ with respect to P . According to (1)-(5) and (10)-(11), $E(P, \rho)$ is the sum of the linear functions $(2-\rho)\rho a W(\rho a, q_r^c)P$ and $(2-\rho)(1-\rho)a W((1-\rho)a, q_h^c)P$, and the nonlinear functions having the form

$$f_6 = (2-\rho)c_1 a P \frac{1-c_1 a}{e^{-\frac{\Gamma}{P}} - c_1 a}. \quad (14)$$

The second derivative of f_6 with respect to P can be easily obtained as

$$f_6'' = (2-\rho)c_1 a(1-c_1 a) \frac{\Gamma^2 e^{-\frac{\Gamma}{P}} (e^{-\frac{\Gamma}{P}} + c_1 a)}{P^3 (e^{-\frac{\Gamma}{P}} - c_1 a)^3}, \quad (15)$$

Based on the constraints, we have $c_1 a < e^{-\frac{\Gamma}{P}}$ for feasible solutions; hence, $f_6'' > 0$ holds, which indicates that f_6 is a convex function of P . Since the sum of linear and convex functions is a convex function, we conclude that the objective function (12a) is a convex function of P . \square

Based on the aforementioned, we propose Algorithm 3 to solve problem (12) in the case of Rayleigh fading. It searches over the domain of P using the Golden section method and at each P , it uses Algorithm 1 to obtain a near-optimal ρ . Therefore, it has the computational complexity of $O(K(\log(1/\delta))^2)$. It is clear that at each iteration, P_1 and P_4 get closer to each other and therefore, the algorithm will terminate finally. As the results in the next section indicate, the proposed algorithm is highly effective and its performance is close to optimum.

IV. NUMERICAL RESULTS

In this section, we verify the presented analysis and also evaluate the performance of the proposed schemes. We consider Rayleigh fading channel on all the links, with $\Gamma_{sr} = \Gamma_{rs} = \Gamma_{rh} = \Gamma_{hr} = 0.01$ corresponding to $\gamma = 10$, $N_0 = 10^{-3}$ and $\bar{g}_{sr} = \bar{g}_{rs} = \bar{g}_{rh} = \bar{g}_{hr} = 1$. The reason for considering similar qualities for all the links is to have equal channel service probabilities on all the links; this enables us to accurately investigate the effect of other deciding factors on

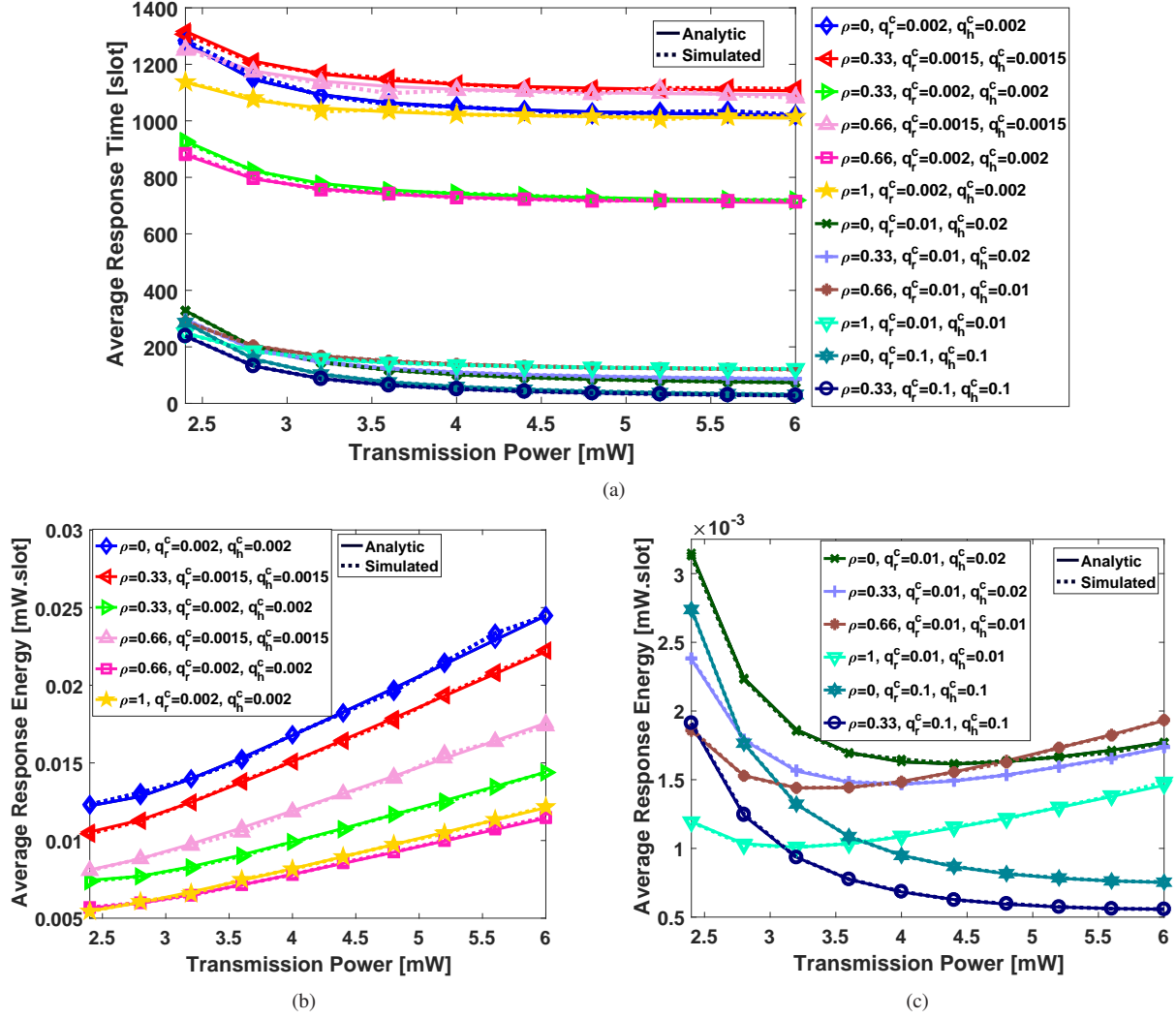


Fig. 3: Analytic and simulation results for (a) ART (b, c) ARE, vs. P ; $a = 0.001$.

the system performance and observe the result of interplay between transmission and computation queues. Hence, we consider several settings for other parameters, as presented in the sequel.

First, we investigate the validity of the analytic results using Matlab simulations for 10^9 time slots. Fig. 3 displays the ART and the ARE with respect to the transmit power in a system with the task arrival probability $a = 0.001$ and different values for ρ , q_r^c , and q_h^c . These settings have been chosen to illustrate different possible patterns of the results, in particular with the MARE scheme. It is observed that the simulation results confirm the analytical results. Moreover, we note that the ART in Fig. 3a decreases as P increases; the RoD in the ART is large at low values of P but small at high values of P . This is in agreement with the analysis presented in the previous section. Also, as expected, the higher the q_r^c and/or q_h^c , the lower the ART. Note that at low values of q_r^c and q_h^c , the ART in the cases with $\rho = 0.33$ and $\rho = 0.66$ is considerably lower than that in the cases with $\rho = 0$ and $\rho = 1$. However, at higher values of q_r^c and q_h^c , either there is a slight difference, or the ART in the cases with $\rho = 0$ or $\rho = 1$ is lower. These indicate

that distributing the tasks between the RS and the HS helps to reduce the ART, when the RS and the HS have lower probabilities of processing the tasks of the SS; but distributing the tasks may not change or may even increase the ART when the probability of task processing at the RS and/or the HS is high.

On the other hand, the ARE has different trends. In order to illustrate them clearly and distinguish different charts, we have shown the results for ARE in Fig. 3b and Fig. 3c. It is observed that as P increases, the ARE may increase, decrease or it may decrease first and then increase. This is because, depending on the system settings and due to the effect of several buffers, the RoI in the SAP and RoD in the ART may be different as P increases. Specifically, at low values of q_r^c and q_h^c shown in Fig. 3b, the queues in the computation buffers are large and the ART is so high that increasing the transmit power does not lead to as much RoD in the ART as the RoI in the SAP; therefore, the ARE is minimum at the lowest P . At moderate values of q_r^c and q_h^c shown in Fig. 3c, the size of the queues in the computation and transmission buffers are close to each other; hence, as P increases, the RoI in the SAP is comparable with the RoD in the ART and consequently, the minimum ARE

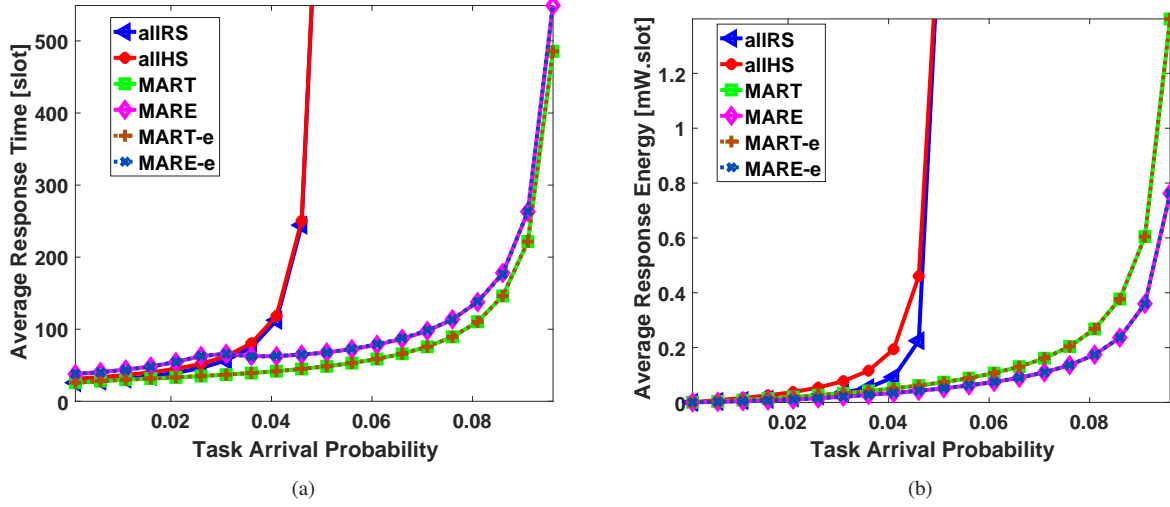


Fig. 4: Effect of task arrival probability a on the (a) ART (b) ARE; $q_r^c = 0.05$, $q_h^c = 0.05$.

happens at a P between the minimum and maximum. At high values of q_r^c and q_h^c , the queues of tasks in the computation buffers are very small and the transmission queues have more influence on the ART; as P increases, the RoD in the ART is more than the RoI in the SAP and therefore, the ARE is minimum at the highest P .

Next, we investigate the performance of the proposed schemes in comparison with allRS and allHS baseline schemes, which refer to the methods where all the tasks are assigned respectively to the RS and to the HS. In both of allRS and allHS, the maximum power is used for transmissions. For the proposed algorithms, we have considered $\delta = 0.0001$ and $K = 1$ and have also compared them with the exhaustive search methods MART-e and MARE-e. In the MART-e and MARE-e methods respectively, the MART and MARE problems are solved by exhaustive search over the domains of P and ρ in steps of δ . The task arrival probability a is considered from 0.001 to 0.096 in steps of 0.005 and the maximum transmit power of the nodes is 10 mW. Note that if the maximum power is used for transmissions, channel service probabilities will be approximately equal to 0.368, which is high above the range of a and will prevent large queuing at the transmission buffers. Hence, in order to guarantee the system stability with the allRS and allHS schemes at least at the beginning (low values of a), we consider both q_r^c and q_h^c equal to 0.05. As shown in Fig. 4, at all values of a , the MART scheme has the lowest ART whereas the MARE scheme has the lowest ARE. This also holds in the results presented later and indicates that the proposed methods are highly effective in reaching their goals to minimize the ART or the ARE. The allRS and allHS schemes have a small ART and ARE when a is lower than 0.02. However, as a increases over 0.02, the ART and ARE with allRS and allHS increase rapidly and then go towards infinity at around $a = 0.045$, whereas this happens for MART and MARE at around $a = 0.096$. This indicates that both MART and MARE optimize the use of transmit power and the processing capabilities at the RS and HS, and result in considerably better performance compared with allRS

and allHS. Moreover, it is observed that, even with $K = 1$, the proposed algorithms achieve almost the same performance as the exhaustive search methods. This has been tested for the scenarios in the sequel, too, and confirms the discussions presented in Remark 1 in the previous section. Hence, to have clear figures in the following, we do not illustrate the results of exhaustive search, and only provide the results obtained by the proposed algorithms and focus on the possible trends.

In order to investigate the performance of the proposed methods in various system settings and provide insights on different trends, we first consider a case with low computation capability at the RS. We fix q_r^c at 0.001 and investigate the effect of task arrival probability in the scenarios with different values of q_h^c . Fig. 5 shows the results, where due to the space shortage, all the sub-figures share the same legend. It is clear in Figs. 5a and 5b that as a goes over 0.06, the ART and ARE increase rapidly in the cases of low q_h^c , i.e., 0.09 and 0.1. Particularly, in the case of $q_h^c = 0.09$, the MART and MARE problems are not feasible when a goes beyond 0.9, which is why the results are not illustrated at $a = 0.91$ and $a = 0.96$. We observe in Fig. 5c that in almost all the considered scenarios, ρ^* is 0 which means all the tasks are computed at the HS; it is only at high a and lower values of q_h^c that ρ^* is a little higher than 0. This trend is due to the fact that when the computation capability is low at the RS, using its computation server will cause large queuing at the RS computation buffer and consequently, high ART in the system. On the other hand, the computation capability is high at the HS and offloading all the tasks to it leads to a lower ART, except for the cases with high a and lower values of q_h^c which necessitate having few tasks processed at the RS. Fig. 5d shows that while with the MART scheme, the maximum power is used for transmissions at the nodes, the MARE scheme achieves comparable ART using different power values. Specifically, at lower values of q_h^c , when a increases from zero to relatively moderate values, the MARE scheme increases P^* as its impact is considerable on decreasing the ART. However, when a increases more, increasing the transmit power does not help

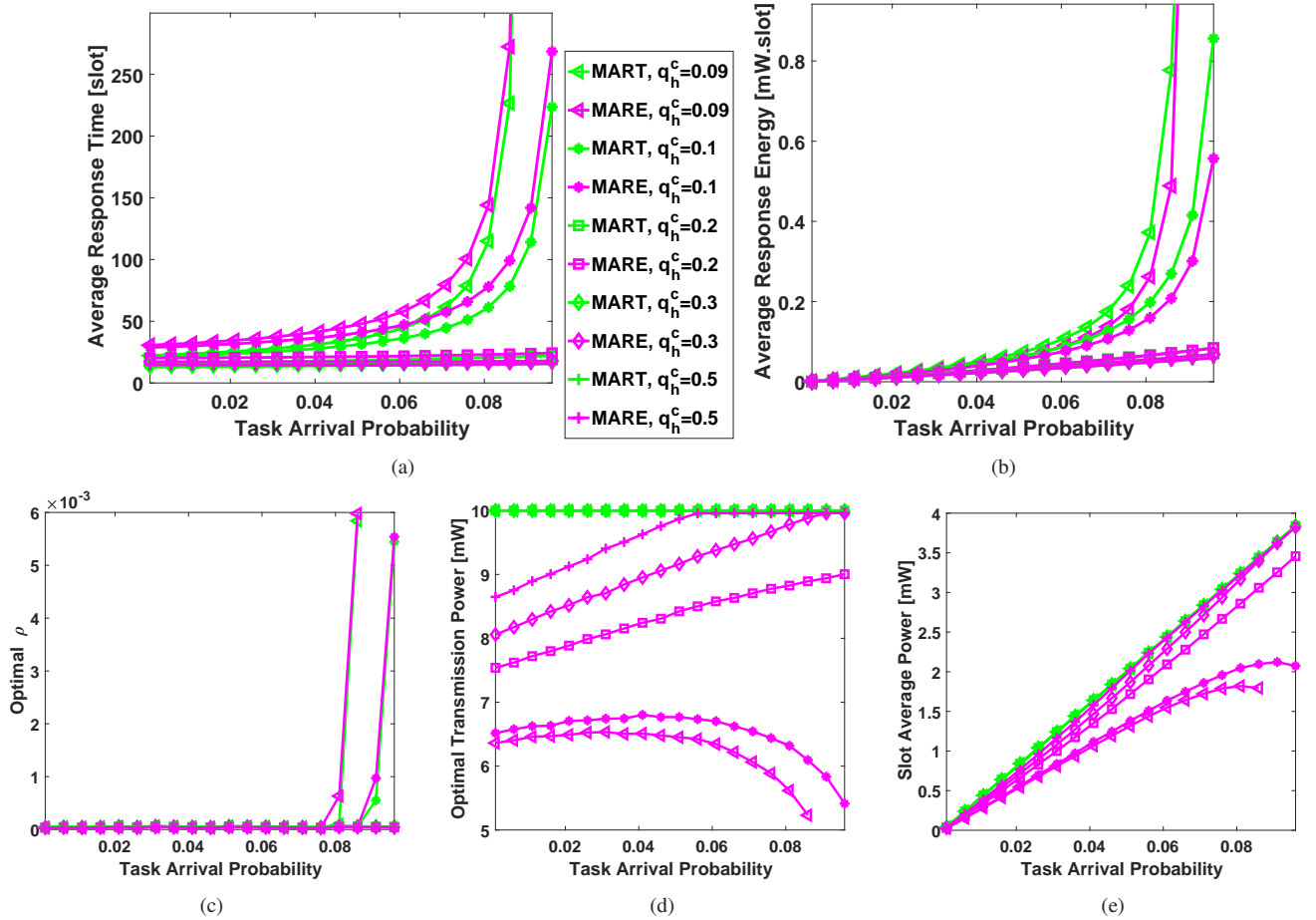


Fig. 5: Effect of task arrival probability a on the (a) ART (b) ARE (c) ρ^* (d) P^* (e) SAP; $q_r^c = 0.001$.

much in decreasing the ART; thus, MARE reduces P^* to save energy, which is reflected on the SAP in Fig. 5e. On the other hand, at high values of q_h^c , as a increases, MARE uses higher transmit power (even up to the maximum, if needed) because its impact on the RoD in the ART is considerable compared with the RoI in the SAP. This is why we also observe that the more the q_h^c , the higher the P^* . Fig. 5e illustrates that the SAP of both MART and MARE increases with task load, which is expected because the more the a , the more the task transmissions on the links and the more the power consumption. Moreover, based on the stated discussions earlier, lower SAP is expected for MARE which is confirmed by the results. Since the energy consumption in the system is directly proportional to the SAP and the number of slots the system runs, it can be inferred that as time passes, the MARE scheme can result in remarkable energy saving in the system.

Next, we fix q_h^c at a relatively high value, i.e., 0.1, and consider different values for q_r^c , from moderate to relatively high, and investigate the effect of increasing the task load. It is observed in Figs. 6a and 6b that at higher values of a , as it increases, the ART and ARE of both the MART and MARE schemes increase continuously towards infinity after some point which is the sign of infeasibility of the MART and MARE problems and instability of the system queues at high task load. The more the q_r^c , the larger the range of a at

which the system queues are stable; this can also be noticed from Figs. 6c, 6d, and 6e. Figs. 6a and 6c indicate that at low task loads, MART achieves the minimum ART by computing all the tasks at the HS ($\rho^* = 0$) or the RS ($\rho^* = 1$) respectively in the case of moderate or high q_r^c . However, as the load increases, ρ^* changes and the tasks are distributed between the RS and the HS, and the more the q_r^c , the more the ρ^* . It is also observed in Figs. 6d and 6e that even though MART uses maximum power at the nodes, the SAP is different for different values of q_r^c . This is due to the fact that the lower the q_r^c , the higher the portion of tasks offloaded to the HS and therefore, the higher the average power consumption in each slot. Also note that when $\rho^* = 1$, task/result transmissions happen only between SS and RS which is why the SAP has a lower slope in the corresponding cases. Fig. 6a shows that the interesting things happen with the MARE scheme at low values of a ; as a increases, the ART increases up to some point and then returns and decreases. The lower the q_r^c , the lower the a and the higher the ART at the return point. These return points correspond to the points in Fig. 6c where ρ^* changes from 1 to a lower value and the points in Fig. 6d where P^* has rapid increase. Their affect is also clear on the SAP in Fig. 6e. This trend is because the RS has a moderate computation capability and MARE tries to assign all the tasks to the RS in order to

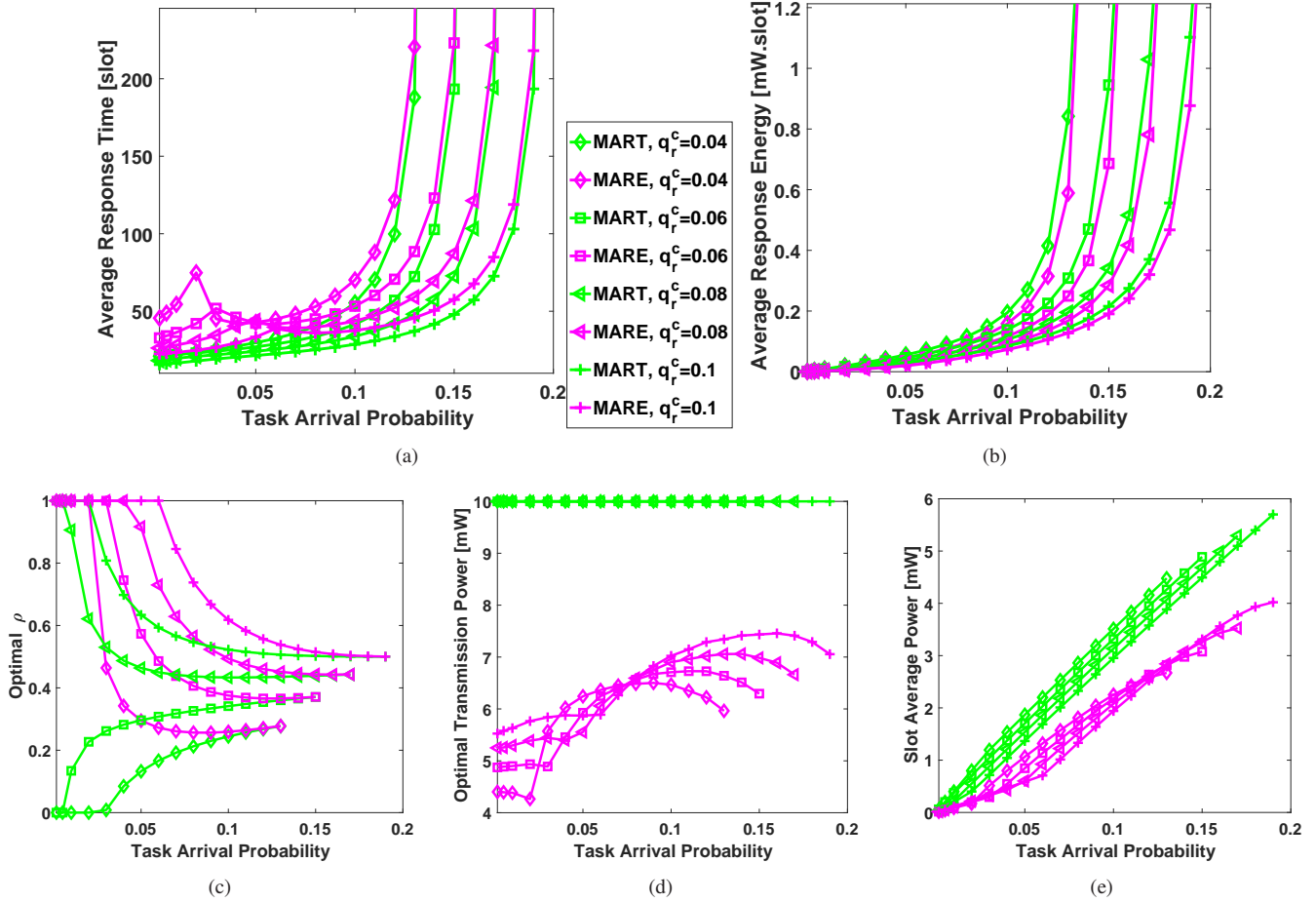


Fig. 6: Effect of task arrival probability a on the (a) ART (b) ARE (c) ρ^* (d) P^* (e) SAP; $q_h^c = 0.1$.

not consume power for RS-HS/HS-RS transmissions of the tasks/results. In fact, at lower loads, MARE does not find the RoD in the ART worth the RoI in the SAP. But, that does not hold as the load increases and therefore, it becomes necessary to offload some tasks to the HS. Now, at this situation, the lower the q_r^c , the lower the ρ^* , and MARE finds the RoI in the SAP worth the RoD in the ART and hence, the transmit power at the nodes are increased. However, as a increases more and the ART increases rapidly, MARE decreases the transmit power, similar to the trends in Fig. 5d discussed previously.

In the previous figures, we observed that as the task load increased, ρ^* was either not changed or it changed smoothly between 0 and 1. Similarly, the changes in P^* was smooth. It is interesting to note that this might not be the case in some system settings. To show that, we consider scenarios with very high computation capability at the HS, i.e., $q_h^c = 0.99$ and moderate to high capabilities for the RS, i.e., q_r^c from 0.05 to 0.5. Since the maximum possible channel service probabilities (i.e., at the maximum power) are approximately 0.368, the ART and the ARE will increase rapidly if the value of a gets close to that. Therefore, we consider a up to 0.3 to be able to show the details at the lower values of a clearly. Fig. 7 shows that the results of MART have trends similar to the ones in the previous figures, but the results of MARE are even more

interesting than those shown before. Here, Fig. 7a indicates that in the cases of q_r^c equal to 0.05 and 0.07 at low a , the ART of MARE has sharp decrease after increase. This can be explained by the sharp change of ρ^* from 1 to 0 in Fig. 7c and the sharp change of P^* from around 5 mW to almost 10 mW in Fig. 7d, as follows. At low a , MARE does not find the RoD in the ART worth the RoI in the SAP and achieves lower ARE by assigning all the tasks to the RS. However, when a increases over a specific value, MARE needs to reduce the load of the RS computing server but it finds that in the new situation, offloading all the tasks to the HS leads to a lower ARE compared with the case of distributing the tasks between the RS and HS. Since the delay at the computation buffer of the HS is very low, the delays at the HS-RS and RS-HS transmission buffers are the deciding factor; hence, a transmit power close to the maximum is used at the nodes to decrease the ART and keep the ARE low. Then, as a increases more, MARE needs to reduce the load of the RS-HS and HS-RS transmission buffers and hence, some tasks are assigned to the RS again. Note that in the case of $q_r^c = 0.5$ with MARE, ρ^* is 1 for all the values of a . In our simulations, we have observed that this remains so and MARE does not distribute the tasks between the RS and HS, even if we increase a over 0.3 and up to the points that the ART gets very high and goes

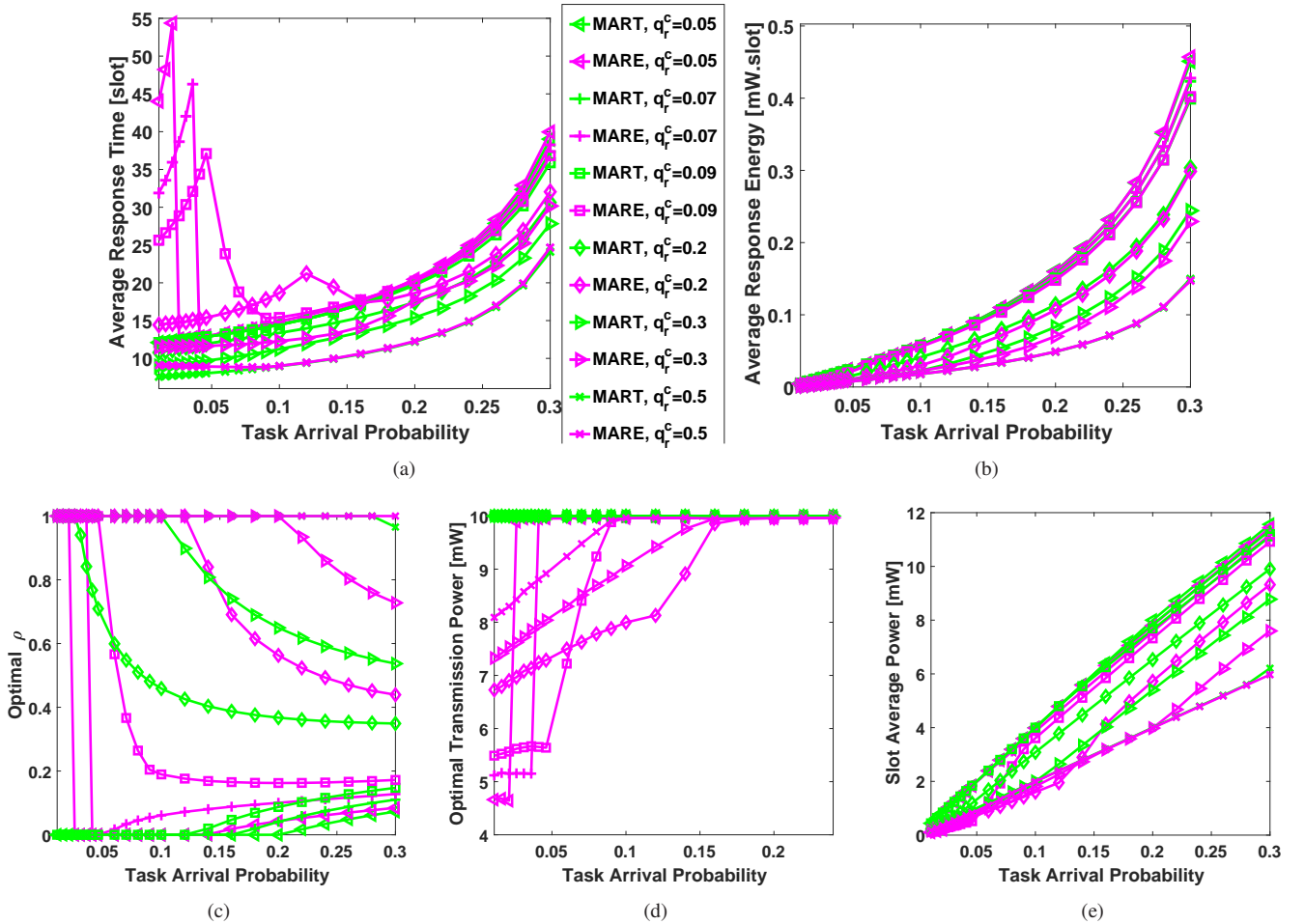


Fig. 7: Effect of task arrival probability a on the (a) ART (b) ARE (c) ρ^* (d) P^* (e) SAP; $q_h^c = 0.99$.

towards infinity. This is due to the fact that the maximum service probability of the transmission buffers is 0.368, and the SS-RS and RS-SS links are the bottlenecks and will cause high ART if a goes over 0.3. Moreover, even though the HS computation probability is 0.99, power consumption for offloading some tasks to the HS at high a is not worth the decrease in the ART due to the large queuing in the RS-HS and HS-RS transmission buffers. Since $q_r^c = 0.5$ is large enough to result in small queuing at the RS computation buffer, assigning all the tasks to the RS leads to lower ARE overall.

V. CONCLUSION

This paper has investigated MMEC in the time-slotted systems with block fading channels and fixed transmit power at the nodes. We have considered stochastic offloading scheme in a system with an SS, an RS, and an HS, where SS sends its tasks to the RS and the RS randomly decides to process the received tasks by its own computing server or to forward them to be processed at the HS. We have provided a framework which takes into account the effect of all the transmission and computation buffers in the system and, exploiting the queuing theory, we have characterized the ART of the system. We have also proposed the concept of the ARE, as the product of the SAP and the ART, which

provides a novel viewpoint about energy efficiency. In order to minimize the ART or the ARE, we have proposed the MART and MARE schemes with the corresponding problem formulations and have analyzed their feasible sets and the objective functions. Based on that, we have presented solution methods and have evaluated their performances. Numerical results confirm the validity of the presented analysis and show that the proposed schemes significantly improve the ART and ARE compared with the baseline methods. Moreover, through the extensive evaluations, we have shown the possible trends in the outcomes of the proposed schemes in different scenarios.

REFERENCES

- [1] W. Shi, J. Cao, Q. Zhang, Y. Li, and L. Xu, "Edge computing: vision and challenges," *IEEE Internet Things J.*, vol. 3, no. 5, p. 637–646, Oct. 2016.
- [2] Y. Mao, C. You, J. Zhang, K. Huang, and K. B. Letaief, "A survey on mobile edge computing: The communication perspective," *IEEE Commun. Surveys Tuts.*, vol. 19, no. 4, p. 2322–2358, Aug. 2017.
- [3] F. Liu, G. Tang, Y. Li, Z. Cai, X. Zhang, and T. Zhou, "A survey on edge computing systems and tools," *Proc. IEEE*, vol. 107, no. 8, pp. 1537–1562, Aug. 2019.
- [4] A. Kiani and N. Ansari, "Toward hierarchical mobile edge computing: An auction-based profit maximization approach," *IEEE Internet Things J.*, vol. 4, no. 6, pp. 2082–2091, Dec. 2017.
- [5] Q. Fan and N. Ansari, "Workload allocation in hierarchical cloudlet networks," *IEEE Commun. Lett.*, vol. 22, no. 4, pp. 820–823, Apr. 2018.

- [6] Z. Chu, P. Xiao, M. Shojafar, D. Mi, J. Mao, and W. Hao, "Intelligent reflecting surface assisted mobile edge computing for internet of things," *IEEE Wireless Commun. Lett.*, pp. 1–1, Nov. 2020.
- [7] F. Zhou, C. You, and R. Zhang, "Delay-optimal scheduling for IRS-aided mobile edge computing," *IEEE Wireless Commun. Lett.*, pp. 1–1, Dec. 2020.
- [8] Y. Dai, D. Xu, S. Maharjan, and Y. Zhang, "Joint load balancing and offloading in vehicular edge computing and networks," *IEEE Internet Things J.*, vol. 6, no. 3, pp. 4377–4387, Jun. 2019.
- [9] G. Wang and F. Xu, "Regional intelligent resource allocation in mobile edge computing based vehicular network," *IEEE Access*, vol. 8, pp. 7173–7182, Jan. 2020.
- [10] C. Guo, W. He, and G. Y. Li, "Optimal fairness-aware resource supply and demand management for mobile edge computing," *IEEE Wireless Commun. Lett.*, pp. 1–1, Dec. 2020.
- [11] C. You, K. Huang, H. Chae, and B. Kim, "Energy-efficient resource allocation for mobile-edge computation offloading," *IEEE Trans. Wireless Commun.*, vol. 16, no. 3, pp. 1397–1411, Mar. 2017.
- [12] Y. Dai, D. Xu, S. Maharjan, and Y. Zhang, "Joint computation offloading and user association in multi-task mobile edge computing," *IEEE Trans. Veh. Technol.*, vol. 67, no. 12, pp. 12313–12325, Dec. 2018.
- [13] H. Sun, F. Zhou, and R. Q. Hu, "Joint offloading and computation energy efficiency maximization in a mobile edge computing system," *IEEE Trans. Veh. Technol.*, vol. 68, no. 3, pp. 3052–3056, Mar. 2019.
- [14] M. T. Kabir and C. Masouros, "A scalable energy vs. latency trade-off in full-duplex mobile edge computing systems," *IEEE Trans. Commun.*, vol. 67, no. 8, pp. 5848–5861, Aug. 2019.
- [15] N. Zlatanov, R. Schober, and P. Popovski, "Buffer-aided relaying with adaptive link selection," *IEEE J. Sel. Areas Commun.*, vol. 31, no. 8, pp. 1530–1542, Aug. 2013.
- [16] N. Zlatanov and R. Schober, "Buffer-aided relaying with adaptive link selection-fixed and mixed rate transmission," *IEEE Trans. Info. Theory*, vol. 59, pp. 2816–2840, May 2013.
- [17] J. Hajipour, R. Ruby, A. Mohamed, and V. C. M. Leung, "Buffer-aided relaying improves both throughput and end-to-end delay," *EURASIP J. Wireless Commun. Netw.*, pp. 1–17, Dec. 2015.
- [18] J. Hajipour, J. M. Niya, and D. W. K. Ng, "Energy-efficient resource allocation in buffer-aided wireless relay networks," *IEEE Trans. Wireless Commun.*, vol. 16, no. 10, pp. 6648–6659, Oct. 2017.
- [19] S. L. Lin and K. H. Liu, "Relay selection for cooperative relaying networks with small buffers," *IEEE Trans. Veh. Technol.*, vol. 65, no. 8, pp. 6562–6572, Aug. 2016.
- [20] J. Hajipour, "Stochastic buffer-aided relay-assisted MEC," *IEEE Commun. Lett.*, vol. 24, no. 4, pp. 931–934, Jan. 2020.
- [21] M. Neely, *Stochastic Network Optimization with Application to Communication and Queueing Systems*. Morgan & Claypool, 2010.
- [22] L. Lakatos, L. Szeidl, and M. Telek, *Introduction to Queueing Systems with Telecommunication Applications*. Springer, 2013.
- [23] D. Bertsekas, *Nonlinear Programming*. Athena Scientific, 1995.